Chen *et al.*
Journal of NeuroEngineering and Rehabilitation (2025) 22:60
https://doi.org/10.1186/s12984-025-01595-y

Journal of NeuroEngineering and Rehabilitation

RESEARCH

Open Access

A motor unit action potential-based method for surface electromyography decomposition

Chen Chen[1*], Dongxuan Li[1] and Miaojuan Xia[1]

Abstract

Objective Surface electromyography (EMG) decomposition is crucial for identifying motor neuron activities by analyzing muscle-generated electrical signals. This study aims to develop and validate a novel motor unit action potential (MUAP)-based method for surface EMG decomposition, addressing the limitations of traditional blind source separation (BSS)-based techniques in computation complexity and motor unit (MU) tracking.

Methods Within the framework of the convolution kernel compensation algorithm, we developed a MUAP-based decomposition algorithm by reconstructing the MU filters from MUAPs and evaluated its performance using both simulated and experimental datasets. A systematic analysis was conducted on various factors affecting decomposition performance, including MU filter reconstruction methods, EMG covariance matrices, MUAP extraction techniques, and extending factors. The proposed method was subsequently compared to representative BSS-based techniques, such as convolution kernel compensation.

Main results The MUAP-based method significantly outperformed traditional BSS-based techniques in identifying more MUs and achieving better accuracy, particularly under noisy conditions. It demonstrated superior performance with increased signal complexity and effectively tracked motor units consistently across decompositions. In addition, directly applying the MU filters reconstructed from MUAPs to decomposition exhibited marked computational efficiency.

Conclusion and significance The MUAP-based method enhances EMG decomposition accuracy, robustness, and efficiency, offering reliable motor unit tracking and real-time processing capabilities. These advancements highlight its potential for clinical diagnostics and neurorehabilitation, representing a promising step forward in non-invasive motor neuron analysis.

Keywords Electromyography decomposition, Motor unit action potential, Neural decoding, Blind source separation, Motor unit tracking

Introduction

Electromyography (EMG) decomposition is a pivotal technique for noninvasively identifying motor neuron activities by analyzing the electrical signals generated by muscle contractions [1, 2]. This technique holds significant potential for various applications, including neurorehabilitation, prosthetic control, and the diagnosis of neuromuscular disorders [3–5]. By providing insights into the functioning of individual motor units (MUs), EMG decomposition can enhance our understanding of motor control and aid in developing advanced biomedical devices [6, 7].

Current EMG decomposition techniques include a variety of methods, with blind source separation (BSS)-based decomposition being one of the most prevalent [8]. BSS-based methods operate on the principle that the

*Correspondence:
Chen Chen
cedric_chen@sjtu.edu.cn
[1] State Key Laboratory of Mechanical System and Vibration, School of Mechanical Engineering, Shanghai Jiao Tong University, Shanghai 200240, China

observed EMG signals are mixtures of signals from multiple sources, in this case, individual motor units. These methods utilize statistical techniques to separate the mixed signals into their original components without prior knowledge of the sources or the mixing process [9]. Common BSS algorithms include fast Independent Component Analysis (fastICA) and convolution kernel compensation (CKC) [10–13], along with their variants. These techniques have shown promising results in accurately decomposing EMG signals under controlled conditions and could effectively separate motor unit discharges and their motor unit action potentials (MUAPs) from surface EMG signals[14, 15]. However, these BSS-based techniques are complex and computationally intensive, posing challenges for real-time applications. In addition, they are highly sensitive to noise and signal cross-talk, which can degrade their performance in less controlled environments [16, 17].

Identifying motor unit discharges across different decompositions is critical for accurate motor unit tracking and analysis. However, current BSS algorithms often struggle to consistently and accurately identify motor unit discharges [18]. This limitation hampers the practical utility of these techniques in myoelectric control or clinical settings, where consistent and reliable motor unit identification is crucial. Current methods for tracking motor units over time typically involve correlating the MUAP shapes and discharge patterns across different recording sessions [19, 20]. These tracking methods, however, often face challenges such as variability in signal quality, changes in electrode positioning, and the inherent non-stationarity of EMG signals. Techniques such as template matching and clustering have been used to track MUAPs, but their reliability can be compromised under varying conditions [21]. Thus, developing a robust and accurate motor unit tracking method for EMG decomposition remains a significant challenge.

In CKC-based decomposition, the cross-correlation vector between sources (motor unit spike train, MUST) and recordings (EMG signals), which is also called a MU filter, is used to filter the matrix-transformed EMG signals to estimate the spike train [9, 22, 23]. The cross-correlation vector is generally calculated by iteration, which is time-consuming and depends on the statistical properties of the decomposed EMG signals. As the MUST is a sequence containing only 0 and 1, the definition of the MU filter is similar to that of the MUAP (detailed explanation can be found in section). Therefore, it might be possible to reconstruct the MU filter from MUAP for EMG decomposition directly. Compared with the cross-correlation vector, the MUAP also represents the unique electrical activity of individual motor units and can be extracted from surface EMG signals [24]. Using MUAP-based methods for EMG decomposition can potentially overcome some limitations of BSS-based techniques. The distinct shapes of MUAPs allow for the identification and tracking of motor unit activities. Additionally, MUAP-based decomposition can be less dependent on the decomposed dataset, making it more applicable in real-world scenarios.

So far, only the separation vectors pre-trained by iteration have been used to directly decompose EMG signals [16, 25, 26], while the decomposition performance of the MUAP-based method remains unknown. Inspired by the CKC algorithm [9][27], we aim to develop and validate a novel method for surface EMG decomposition based on MUAPs. Based on the assumption of distinctiveness among MUAPs, we leverage the unique characteristics of MUAPs and seek to improve the accuracy and reliability of EMG decomposition and MU tracking, thereby enhancing its utility for both clinical and research applications. This study will assess the performance of the proposed method and compare it with existing techniques, highlighting its potential advantages and applications.

Methods

Decomposition algorithm

The EMG signals are generally modeled as a multi-input-multi-output system [12]:

$$x_i(n) = \sum_{j=1}^{J} \sum_{l=0}^{L-1} h_{ij}(l)\theta_j(n-l) + w_i(n), i = 1, 2, ..., M \tag{1}$$

where x_i denotes the EMG signal from ith channel, n is the sample point, θ_j is the pulse train of the jth MU and h_{ij} is the corresponding pulse response (action potential waveform), L is the sample length of the action potentials, w_i is the additive noise signal for the ith channel, and J and M are the numbers of active MUs and EMG channels, respectively.

The Eq. 1 can be reformed as:

$$x = H\theta + w \tag{2}$$

where H is the mixing matrix containing the pulse response of active MUs, and $\theta = E(x\theta^T) = [\theta_1(n), \theta_1(n-1), ..., \theta_1(n-L+1), ..., \theta_J(n), ..., \theta_J(n-L+1)]^T$ is the extended version of the all pulse trains [12]. The mixing model denoted by Eq. 2 is similar to a Bayesian linear model. As the mathematical expectation of EMG (x) and pulse trains (θ) are close to zero, the LMMSE estimations of the pulse train can be written as [28]:

$$\hat{\theta} = C_{\theta x}^T C_{xx}^{-1} x \tag{3}$$

where $C_{\theta x} = [c_{\theta_1 x}, c_{\theta_2 x}, ..., c_{\theta_J x}]$ contains the cross-correlation vector between each pulse train and EMG signals,

and $C_{xx} = E(xx^T)$ is the covariance matrix of EMG signals, E denotes the mathematical expectation.

The CKC algorithms used Eq. 3 to estimate the MUSTs [9], where the $c_{\theta_j x}$ is defined as:

$$c_{\theta_j x} = E(\theta_j x^T) = \lim_{card(\Psi_j)\to\infty} \frac{1}{card(\Psi_j)} \sum_{n_k \in \Psi_j} x(n_k) \tag{4}$$

where Ψ_j is the set containing the discharge timings of the jth MU. To increase the ratio between observation and source, the EMG signals are generally extended by K delays, adding K delayed versions of each observation [11]:

$$\bar{x}(n) = [x_1(n), x_1(n-1), ..., x_1(n-K+1), ...x_M(n), ..., x_M(n-K+1)] \tag{5}$$

By inserting Eq. 5 into Eq. 4, the resulting $c_{\theta_j \bar{x}}$ now reflecting the jth MU's pulse response with a length of K samples.

In the CKC algorithm, the $c_{\theta_j \bar{x}}$ can be estimated iteratively using a natural gradient descent method (gCKC) [27]:

$$\hat{c}_{\theta_j \bar{x}, k+1} = \hat{c}_{\theta_j \bar{x}, k} + l \sum_n \frac{\partial f(\hat{\theta}_j(n))}{\partial \hat{\theta}_j(n)} \bar{x}(n) \tag{6}$$

where $\hat{\theta}_j$ is the jth pulse train estimated depending on Eq. 3 in each iteration, l is the learning rate, $f(x)$ is the cost function. The $\frac{\partial f(x)}{\partial x}$ should be the concave even function [27], which was set as $\frac{\partial f(x)}{\partial x} = t^2$ in this study. The cross-correlation matrix ($C_{\theta x}$) or separation matrix ($C_{\theta x}^T C_{xx}^{-1}$) is often kept to decompose new data [13, 16, 26]. It should be noted that the EMG signals have not been whitened during decomposition.

During BSS-based EMG decomposition, the MUAP waveforms can be extracted by post-processing. The spike-triggered averaging (STA) is one of the most common methods to extract the MUAP waveforms [29]:

$$MUAP_{ij}(n) = \frac{1}{card(\Psi_j)} \sum_{n_k \in \Psi_j} x(n_k - \frac{N}{2} + n), n = 1, 2, ..., N \tag{7}$$

where $MUAP_{ij}$ indicates the jth MU's waveform at channel i with a sample length of N. The calculation of MUAP waveforms depending on Eq. 7 is similar to Eq. 4, especially when the EMG signals are extended. As the sample in a spike train is 1 only when the MU discharges, the $c_{\theta_j x}$ becomes the pulse response of the jth MU. When the EMG signals by K delays, the $c_{\theta_j \bar{x}}$ reflects the pulse response with a duration of K samples, which can be regarded as MUAP in ideal conditions, indicating the possibility of using MUAP waveforms to estimate the MUSTs. Moreover, the sample length, which requires to be pre-defined for $c_{\theta_j \bar{x}}$, is more flexible for MUAP.

Therefore, we proposed a MUAP-based decomposition algorithm as shown in Fig. 1. The EMG signals are initially decomposed into MUSTs using the algorithm described above. The multichannel MUAP for each MUST is subsequently estimated through STA. Portions of the MUAP waveforms are extracted to reconstruct the MU filter. The details of reconstruction are given in section . These MU filters are then utilized to decompose new datasets.

The detailed steps of the proposed MUAP-based decomposition method are shown in Algorithm 1. To test the effect of intermediate parameters in the algorithm and validate the efficiency of the proposed method, we adopted two datasets under simulated and experimental conditions (section). The intermediate steps including MUAP extraction (step 4 in Algorithm 1), MU filter

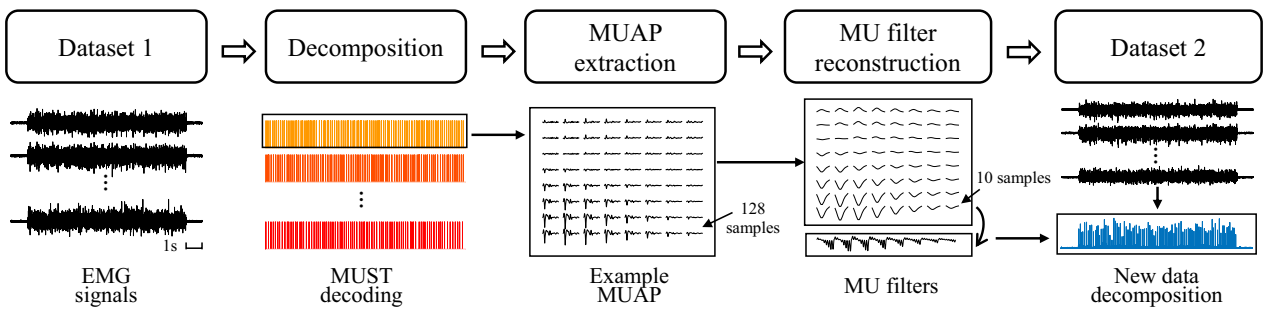

Fig. 1 The flowchart of MUAP-based decomposition. The EMG signals are first decomposed into MUSTs. The multichannel MUAP of each MUST is then estimated by STA. Part of MUAP waveforms from all channels are extracted to reconstruct the MU filter. The obtained MU filters are used to decompose the new dataset

reconstruction (step 5), covariance matrix calculation (step 10), and pulse train estimation (steps 11 and 12) were analyzed as in section .

Algorithm 1 The proposed MUAP-based decomposition method

procedure RECONSTRUCT MU FILTERS
Preprocess the EMG dataset 1, x_1: bandpass filtering, extending, etc.
Decompose x_1 into motor unit discharges with a CKC algorithm, obtaining the MUSTs, $\Theta = [\theta_1, \theta_2, ..., \theta_J]$.
Estimate the multichannel MUAPs of each MUST, $P_1, P_2, ..., P_J$, depeding STA. The waveform duration in each channel of P_j was set as 62.5 ms (128 samples) in this study.
Extract an epoch with K samples from each channel of P_j and cascade them to reconstruct the MU filter, $c_{\theta_j x}$.
Put all the MU filters into $C_{\Theta x}$, $C_{\Theta x} = [c_{\theta_1 x}, c_{\theta_2 x}, ..., c_{\theta_J x}]$.
end procedure

procedure DECOMPOSE NEW DATASET
Preprocess a new EMG dataset, x_2.
Extend x_2 with K samples and calculate the covariance matrix.
(optional) Put $C_{\Theta x}$ as initial values and optimize the MU filters iteratively depending on Eq. 6.
Calculate the LMMSE estimations of pulse trains with reconstructed MU filters ($C_{\Theta x}$), depending on Eq. 3.
Extract the spikes from $\hat{\theta_j}$ by K-means clustering and output the MUSTs.
end procedure

Data collection for validation

Simulated signals

EMG signals were generated in the simulated datasets by convolving the simulated MUSTs with MUAPs. The MUSTs were simulated with recruitment thresholds distributed according to an exponential function, organized by size, as previously modeled in [30]. Each motor unit initially discharged at a frequency of 8 Hz upon recruitment. The discharge rate then increased by 0.3 Hz per percent of excitation until reaching a maximum frequency of 35 Hz [31]. The inter-spike interval (ISI) variability followed a Gaussian distribution with a coefficient of variation (CoV) of 20%, calculated as the standard deviation divided by the mean ISI [13]. The MUAPs were extracted from our previous experiments [25]. The high-density surface EMG signals (8×8 with an inter-electrode distance of 10 mm in the two directions) were recorded during the isometric contraction of wrist movements and decomposed into MUSTs by CKC. The MUAPs were extracted using the STA after EMG decomposition. When selecting MUSTs for MUAP extraction, relatively strict thresholds were adopted to ensure the decomposition accuracy, where only MUSTs with pulse-to-noise ratio (PNR) >30dB and CoV<0.3 were used to extract the MUAPs. No manual adjustments were implemented for MUSTs. Each MUAP consists of 64 channels of 62.5-ms waveforms with a sampling rate of 2048 Hz. Finally, we constructed a library containing 700 MUAPs.

We simulated five datasets, each containing six MU groups. Each MU group consisted of 20 MUs. The MUSTs in each group were generated based on the model described above. For each MU group, we only simulated the condition under constant excitation, where all the MUs were activated, but their firing rates differed. The MUAPs in each dataset were first randomly selected from the MUAP library (120 out of 700) and divided into six groups. In a simulation trial, the MU groups were gradually activated every 12 s, from only one active group to six. Each trial can be divided into seven segments as the first group was individually activated once more to extract the MUAP and MU filters for the following decomposition (Fig. 2). Each dataset includes six trials. In each trial, one out of six MU groups was selected as the first group. There were, in

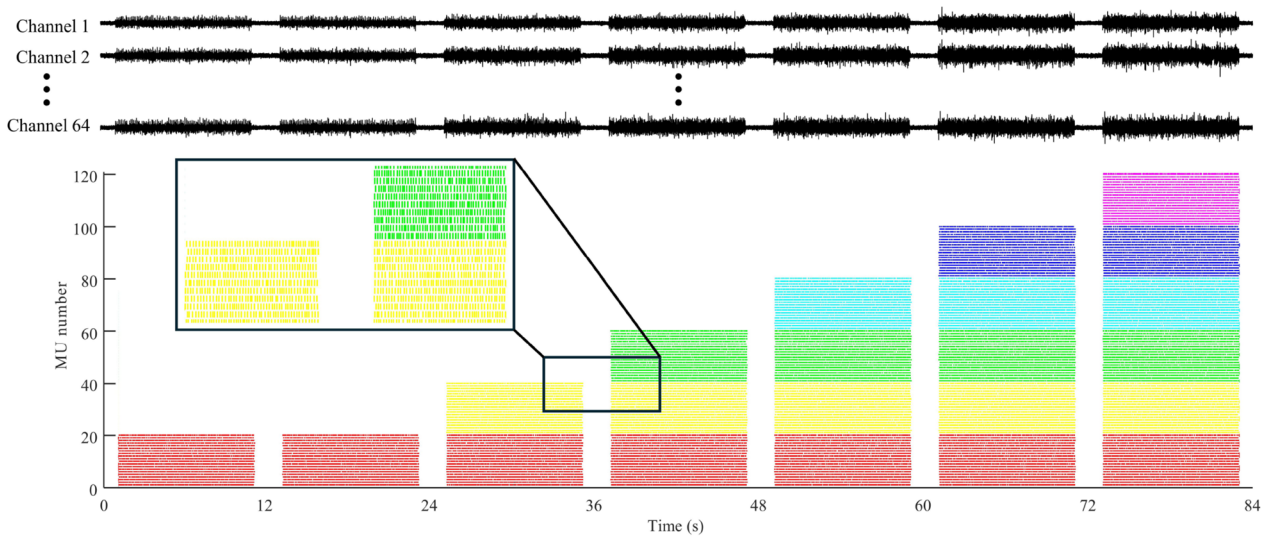

Fig. 2 Example EMG signals and MUSTs in simulation datasets. The EMG signals included seven segments, each lasting for 12 s. The first two segments contain only one MU group, while segments 3–7 contain 2–6 MU groups, respectively. The spike train in each row represents the discharges from the same MU, and each MU group is indicated with one color. The inset shows the zoomed-in simulated MUSTs from adjacent two segments

total, 30 conditions (5 datasets × 6 trials) for simulated signals. For each condition, colored zero-mean Gaussian noise with a signal-to-noise ratio (SNR) of 20 dB, 10 dB, or 0 dB was added to the simulated signals. The whitening noise was added first, and then bandpass filtered between 20 and 500 Hz.

Experimental signals

For the experimental signals, we aimed to test the proposed method's ability to decompose complex EMG signals and thus conducted two experiments. The first experiment involves EMG signals from movements with multiple degrees of freedom (DoF) and combined motions, while the second experiment includes EMG signals at different contraction levels.

In the first experiment, we recruited twelve healthy subjects (nine males and three females, aged 25±3) to perform the isometric contraction of four wrist movements. The detailed experimental configuration can be found in [32]. In short, three electrode grids, each containing 64 channels (8×8, interelectrode distance of 10 mm in both directions, ELSCH064NM3, OT Bioelettronica, Italy), were mounted around the proximal third of the forearm. The EMG signals were amplified and sampled at 2048 Hz with a multi-channel amplifier (EMG-USB2+, OT Bioelettronica, Italy). The EMG signals were recorded in monopolar mode, and A/D converted on 12 bits. The EMG signals were bandpass filtered between 20 and 500 Hz with a 4th-order Butterworth filter. Another comb filter with a cutoff frequency of 50 Hz was implemented to remove power line interference. Few channels with excessive noise, which might be caused by poor contact with skin, were removed before decomposition. The subjects were instructed to perform four individual wrist movements (pronation, supination, flexion, and extension) and their four combinations (pronation+flexion, pronation+extension, supination+flexion, supination+extension). Three repetitive trials were included for each condition, each lasting for 20 s. For individual movements, the subject performed the isometric contraction following a trapezoidal curve. The upper limit of the curve was set as 40% maximum voluntary contraction (MVC) force. For combination movements, the subject performed the two movements following two trapezoidal curves concurrently. There was a delay between the two trapezoidal curves.

In the second experiment, eight healthy subjects (all males, aged 27±5) were recruited and instructed to perform a series of grasping tasks [33]. Four electrode grids of 64 channels (5×13 with 4 mm interelectrode distance in both directions, ELSCH064NM4, OT Bioelettronica, Italy) were mounted on the forearm covering the dominant extensor muscles. The recording configuration was the same as in the first experiment. The grasping force was measured concurrently with

EMG signals by a customed S-shaped transducer. The MVC force was measured first, and the isometric contractions at five different force levels (10%, 30%, 50%, 70%, and 90% MVC) were performed following a trapezoidal curve (1-second ramp-up to the targeted force level, followed by an 8-second flat phase, and a 1-second ramp-down). Each force level included four repetitive four trials. More details about this experiment can be found in [34].

The experimental protocol was approved by the local ethics committee of Shanghai Jiao Tong University (approval number B2020026I) and followed the Declaration of Helsinki.

Data analysis

Decomposition

In each trial of simulated EMG signals, the first 12-s EMG signals were decomposed to obtain the MUAP and MU filters. The MU filters were then used to decompose the remaining EMG signals in this trial. During decomposition, several factors may affect the decomposition performance, such as the ways to extract MUAP and reconstruct MU filters and the EMG covariance matrix used for decomposition. The effect of these factors on the decomposition performance was evaluated based on the simulated EMG signals.

We first tested the decomposition performance when using different ways to reconstruct MU filters from MUAPs (step 5 in Algorithm 1). Generally, the extracted waveforms from MUAPs should capture variations as much as possible to ensure distinction from other MUAPs. Following this principle, we proposed four ways to reconstruct MU filters and tried to find the optimal one. Suppose the sample length of the MU filter in each channel was K and the MUAP in the ith channel (P_i) owned the maximum absolute amplitude among all channels (Fig. 3A), the K samples from each channel, centered by n_0, were determined by the following four methods (Fig. 3B).

- Centered Spike: The K samples around the center of the waveform are extracted. $n_0 = N/2$, where N (128 in this study) is the length of P_i.
- Maximum PPV: The K samples should own the maximum peak-to-peak value (PPV) at channel i. $n_0 = \arg\max f(n_0), f(n_0) = \max(P_i(n_0 - K/2 : n_0 + K/2)) - \min(P_i(n_0 - K/2 : n_0 + K/2))$. If there is more than one case, the n_0 will be set as the center between the maximum and minimum values.
- Maximum Product: The K samples should own the Maximum Product of absolute maximum and minimum value at channel i. $n_0 = \arg\max f(n_0), f(n_0) = |\max(P_i(n_0 - K/2 : n_0 + K/2)) \cdot \min(P_i(n_0 - K/2 : n_0 + K/2))|$. If there is more than one case, the n_0 will be set as the center between the maximum and minimum values. If the distance between the maximum and minimum value is less than K, this method is the same as Maximum PPV.
- Centered Peak: The K samples should be centered around the maximum absolute value of channel i. $n_0 = \arg\max f(n_0), f(n_0) = |P_i(n_0)|$.

The first method (Centered Spike) serves as a baseline, extracting the waveform centered on the decomposed spikes. The second and third methods (Maximum PPV

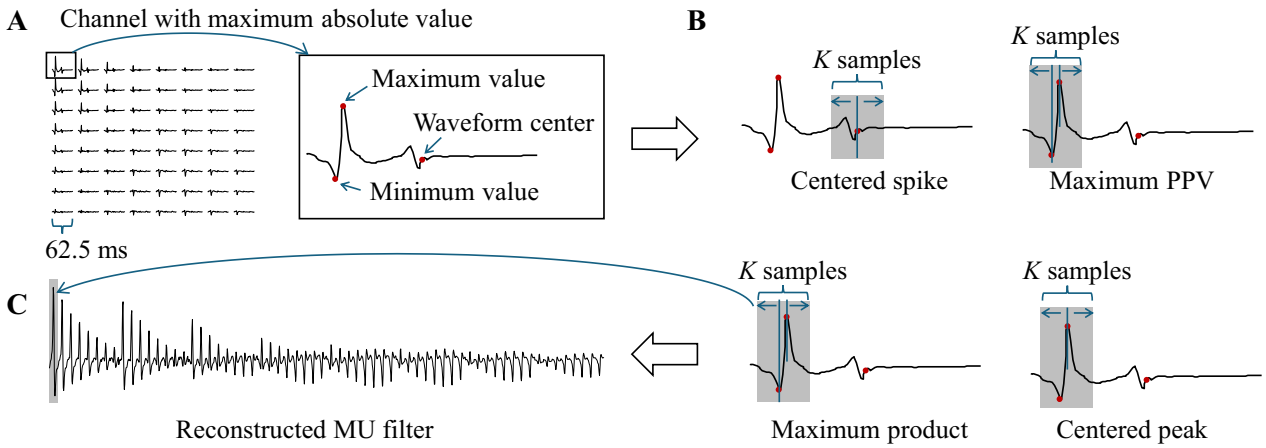

Fig. 3 Illustration of MU filter reconstruction. **A** shows an example of MUAP with 64 channels and the waveform from the channel with the maximum absolute value. The four methods to extract the K samples (in the gray blocks) are illustrated in **B**. If the distance between the maximum and minimum values is less than K samples, the Maximum PPV and Maximum Product will extract the same area in each channel as here. **C** gives the reconstructed MU filter via Maximum Product with $64 \times K$ samples

and Maximum Product) aim to maximize the amplitude variation within the extracted segment, with the distinction that one relies on differences while the other uses products for evaluation. The fourth method assumes that the waveform undergoes the most significant variation at the MUAP's peak amplitude, making it the most representative of the MU's waveform distribution. During this test, the MU filters were reconstructed from ground-truth MUAPs, which were used to simulate the EMG signals.

After extracting K samples from the channel with maximum absolute amplitude (the ith channel), the K samples at the same positions from all remaining channels were also extracted and cascaded to form the MU filter. Figure 3 shows the flowchart of MU filter reconstruction. The K samples from each channel constitute 1/64 of an MU filter (Fig. 3C).

Three types of EMG covariance matrix (C_{xx}) were then tested (step 10 in Algorithm 1). The ground-truth MUAPs were used during this test, and the MU filters were reconstructed based on the Centered Peak method. Suppose x_1 denotes the EMG signals to reconstruct MU filters ($C_{\theta\bar{x}_1}$) and x_2 is the new EMG signals to be decomposed by reconstructed MU filters, the MUSTs ($\hat{\theta}$) are estimated as:

- Raw Cxx: the C_{xx} was calculated based on EMG signals (x_1) used for MU filter reconstruction. $\hat{\theta} = C_{\theta\bar{x}_1} C^{-1}_{\bar{x}_1\bar{x}_1} \bar{x}_2$.
- Current Cxx: the C_{xx} was calculated based on EMG signals (x_2) to be decomposed by MU filters. $\hat{\theta} = C_{\theta\bar{x}_1} C^{-1}_{\bar{x}_2\bar{x}_2} \bar{x}_2$.
- Global Cxx: the C_{xx} was calculated based on all EMG signals ($[x_1, x_2]$) in each trial. $\hat{\theta} = C_{\theta\bar{x}_1} C^{-1}_{[\bar{x_1},\bar{x_2}][\bar{x_1},\bar{x_2}]} \bar{x}_2$.

Two MUAP extraction methods (step 4 in Algorithm 1), STA and least square (LS), were also tested [35]. The STA method extracts the MUAPs depending on Eq. 7. Suppose J MUs were activated and the MUAP had M channels, the LS method estimated the MUAP matrix H as:

$$\hat{H} = (\bar{\theta}^T \bar{\theta}) \bar{\theta}^T \bar{x} \tag{8}$$

where $\bar{\theta}$ is the extended pulse trains with N delays similarly as Eq. 5, $\hat{H}$ (dimension $JN \times M$) contains estimated MUAPs of J MUs at M channels with a sample length of N. For both the STA and LS methods, the duration of MUAP waveforms (N) was set to 62.5 ms (128 samples). During this test, the MU filters were reconstructed based on the Centered Peak method, and the Current Cxx was used for decomposition.

When reconstructing MU filters from MUAPs, different extending factors (K, step 5 in Algorithm 1), ranging from 10 to 60, were also tested with different ways to extract MUAP. The MU filters were reconstructed from ground-truth MUAPs or STA-extracted MUAPs. For the MUAPs extracted by STA, we also implemented a principal component analysis (PCA) to compress the noise and smooth the waveforms [36]. The number of principal components kept for MUAP reconstruction corresponded to >90% of explained variance. The noise might be caused by the original spike train or by a low number of firings where STA has not canceled out all the noise. During this test, the MU filters were reconstructed based on the Centered Peak method, and the Current Cxx was used for decomposition.

At last, different ways to apply the MU filters to MUST estimation were tested (steps 11 and 12 in Algorithm 1).

- MUAP-direct: The MU filters were used to directly estimate the MUSTs depending on Eq. 3.
- MUAP-iteration: The MU filters were used as the initial iteration vector ($\hat{c}_{\theta_j\bar{x},0}$) and estimated depending on Eq. 6.
- MUAP-refine [11, 37]: The MU filters were used as the initial iteration vector and estimated depending on Eq. 4, where Ψ_j is the set containing the pulses estimated in the last iteration.

After MUST estimation, the pulse trains were extracted using the K-means clustering from the $\hat{\theta}$. For comparison with classic decomposition, the separation matrix ($C^T_{\theta x} C^{-1}_{xx}$) was also used to directly decompose the EMG signals, which was denoted as W-direct.

For the EMG signals in the first experiment, the EMG signals recorded during individual movements were decomposed to obtain the MU filters. The MU filters were then used to decompose the EMG signals of movement combinations. As to the second experiment, we first performed separate decompositions for each force level. Based on the decomposition results, MUAPs were extracted to reconstruct MU filters, forming an MU filter library. This library, containing all MU filters, was then used to decompose the signal from all force levels. The decomposition was implemented for each electrode grid, and the MUSTs identified from each grid were combined. The Centered Peak, current Cxx, STA, and MU-direct methods were used to decompose experimental EMG signals.

Duplicate MUSTs might be identified during decomposition. Two MUSTs were considered to belong to the same MU when the rate of agreement (RoA) between

them was higher than 0.3 [38], and only the MUST with the higher PNR was kept.

$$\mathrm{RoA} = \frac{\mathrm{n_{common}}}{\mathrm{n_A} + \mathrm{n_B} - \mathrm{n_{common}}} \quad (9)$$

where n_A and n_B are the number of pulses from the identified and generated MUSTs, and n_{common} is the number of common pulses from the two MUSTs. The time tolerance of two discharges identified from both MUSTs was set to 0.5 ms.

The proposed MUAP-based decomposition method was fully automated, and the obtained MUSTs, whether for MUAP extraction or accuracy evaluation, were entirely free from manual intervention. The MUAP-iteration decomposition was implemented when testing the effect of different methods for MU filter reconstruction, covariance matrix calculation, and MUAP extraction. The extending factor of EMG signals was set to 10. The maximum number of iterations for estimating each MU filter was 45. Iteration stops, and the estimation of the next MUST begins when the maximum number of iterations is reached, or the change in the estimated MUST is less than 1% for two consecutive iterations. The Current Cxx was used to test the MU filter reconstruction methods. Apart from the difference in iteration strategy, the parameter settings for MUAP-refine are identical to those for MUAP-iteration. The gCKC method was also used for EMG decomposition as a control group for both simulation and experimental signals. When implementing the gCKC algorithm, the maximum number of MU filters or MUST estimation was set to 100, while the remaining parameters were kept identical to those used in the MUAP-based method. The time cost of each decomposition method was compared based on an Intel CPU (i7-12700K).

Accuracy evaluation

For the simulated EMG signals, the MU filters reconstructed from the first 12 s, where only one MU group was activated, were used to decompose the EMG signals generated from one to six MU groups. The decoded MUSTs were compared with the ground truth in the first group, as the MU filters were reconstructed from this group. The RoA between the identified MUSTs and ground truth was used to evaluate the decomposition accuracy [38]. Only the MUs with RoA> 0.3 were kept for the following analysis [38].

For the experimental EMG signals, the PNR was used to evaluate the decomposition. Only the MUs with PNR> 25dB were kept for the following analysis. The threshold of PNR was lower than that in the EMG simulation to keep more MUSTs for the following analysis. The discharge rate curve of each MUST during movement combinations was calculated by sliding averaging with a Hanning window. The Pearson correlation coefficient between the discharge rate and torque curves of each movement was calculated. A MUST was regarded as belonging to a motion if the correlation coefficient was higher than 0.7. If a MU did not belong to any motion, this MU would be removed. The kept MUs were regarded as confident due to their high correlation with movements and were counted to evaluate the decomposition efficiency.

A one-way analysis of variance was applied to evaluate the effect of the described factors (MUAP extraction, MU filter reconstruction, C_{xx}, decomposition ways) on the decomposition performance (MU number and RoA). The homogeneity of variance for the variables was first tested. If satisfied, the Bonferroni method was conducted. If not, Dunnett's C method was used instead. The significance level was set to 0.05.

All the simulations, decomposition, and analyses were implemented in MATLAB 2024a (Matlab Inc. USA).

Results

Decomposition accuracy and performance

Figure 4 illustrates the impact of different intermediate steps on the decomposition results. Specifically, the number of identified MUs and their RoA are compared across various methods of MU filter reconstruction, EMG covariance matrix, and MUAP extraction. Among the tested methods, the Centered Peak method yielded the highest number of identified MUs and the best RoA, with significant differences (P<0.001, Fig. 4A). Therefore, we recommend it as the preferred method for extracting MU filters from MUAPs. The decomposition performance varied with different covariance matrices. The Current Cxx and global Cxx methods exhibited comparable decomposition performance, and both significantly outperformed the Raw in terms of the number of identified MUs and RoA (P<0.001) (Fig. 4B). The STA method demonstrated superior performance in MUAP extraction compared to the LS method, achieving higher RoA values and identifying more MUs (Fig. 4C).

Decomposition time cost

The time cost for decomposing 12-second EMG signals using different methods is presented in Tab. 1. The MUAP-direct method exhibited the lowest time cost across all extending factors, ranging from 1.00±0.17s to 1.06±0.15s. In contrast, the MUAP-iteration and gCKC methods required significantly more time, particularly as the extending factor increased, with the gCKC method taking up to 484.77±41.67s for an extending factor of 60.

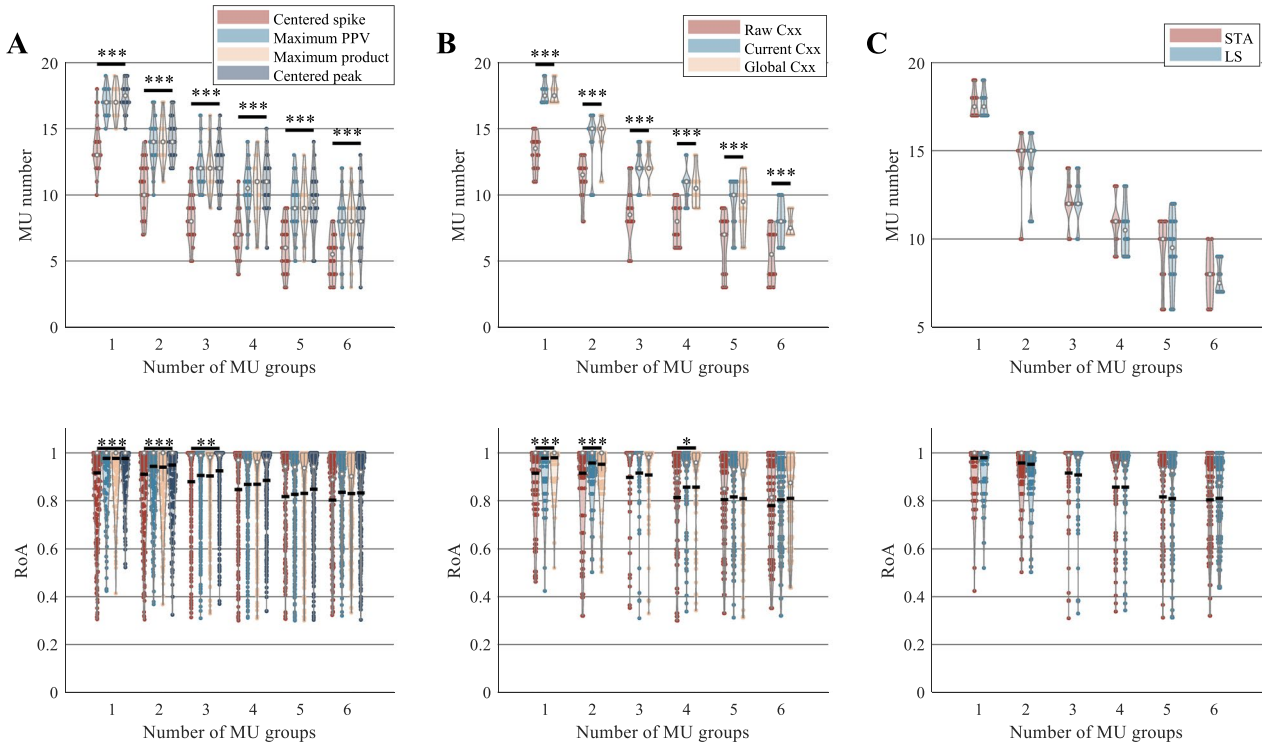

Fig. 4 The effect of different intermediate steps on decomposition results. **A-C** shows the number of identified MUs and their RoA when using different extraction methods for MU filters, covariance matrix, and MUAP, respectively. The number in the horizontal axis indicates how many MU groups were involved when generating EMG signals. The symbols $*$ and $***$ indicate the significant level of $0.01 < P < 0.05$ and $P < 0.001$, respectively. The black horizontal lines in the violin plot of RoA results indicate the mean values. The decomposition results were obtained based on the simulated signals with an SNR of 20 dB

Impact of decomposition methods under different conditions

The performance of different decomposition methods under simulated conditions without noise and with SNR of 20 dB, 10 dB, and 0 dB, is shown in Fig. 5. The MUAP-refine method identified the highest number of MUs and achieved the best RoA, significantly outperforming other methods (P<0.001) (Fig. 5A). Under noisy conditions, the MUAP-refine method continued to perform well, maintaining a higher RoA and identifying more MUs than other methods. In the case of 20 active MUs and a 20 dB SNR, 16.17±1.68 MU filters were successfully identified. Notably, the number of identified MUSTs by gCKC was 16.20±1.65, indicating a success rate close to 100% of MU filter reconstruction. The complexity of EMG signals had a negative effect on the decomposition performance, as the number of identified MUs and RoA decreased when more MU groups were involved. Under 0 dB conditions, few MUs could be identified from all the methods, especially when six groups of MUs are simultaneously activated. This is primarily due to the original gCKC algorithm's limited ability to effectively decode MUSTs and estimate MUAPs. The success rate of MU filters used for MUST decomposition ranges from 36.9% to 100% under 0 dB conditions. Figure 6 shows three examples of MU filter reconstruction and their true values under different noise conditions. Among them, we can effectively reconstruct the MU filter for MU1 and use it for MUST decoding at all noise levels. However, for MU2 and MU3, the 0 dB noise level prevents effective MUAP extraction and MUST decoding, leading to the failure of MU filter reconstruction.

Effect of extending factors

Figure 7 illustrates the effect of varying extending factors on decomposition results when different numbers of MU groups were involved. For MU filters reconstructed from MUAPs using the Centered Peak method, the performance improved with increasing extending factors up to a certain point, after which the benefits plateaued. Using true MUAPs for extraction yielded the highest RoA and number of identified MUs across all extending factors. Both methods showed a similar trend, with performance peaking at an extending factor of 40 and declining slightly thereafter. For the gCKC method, the number

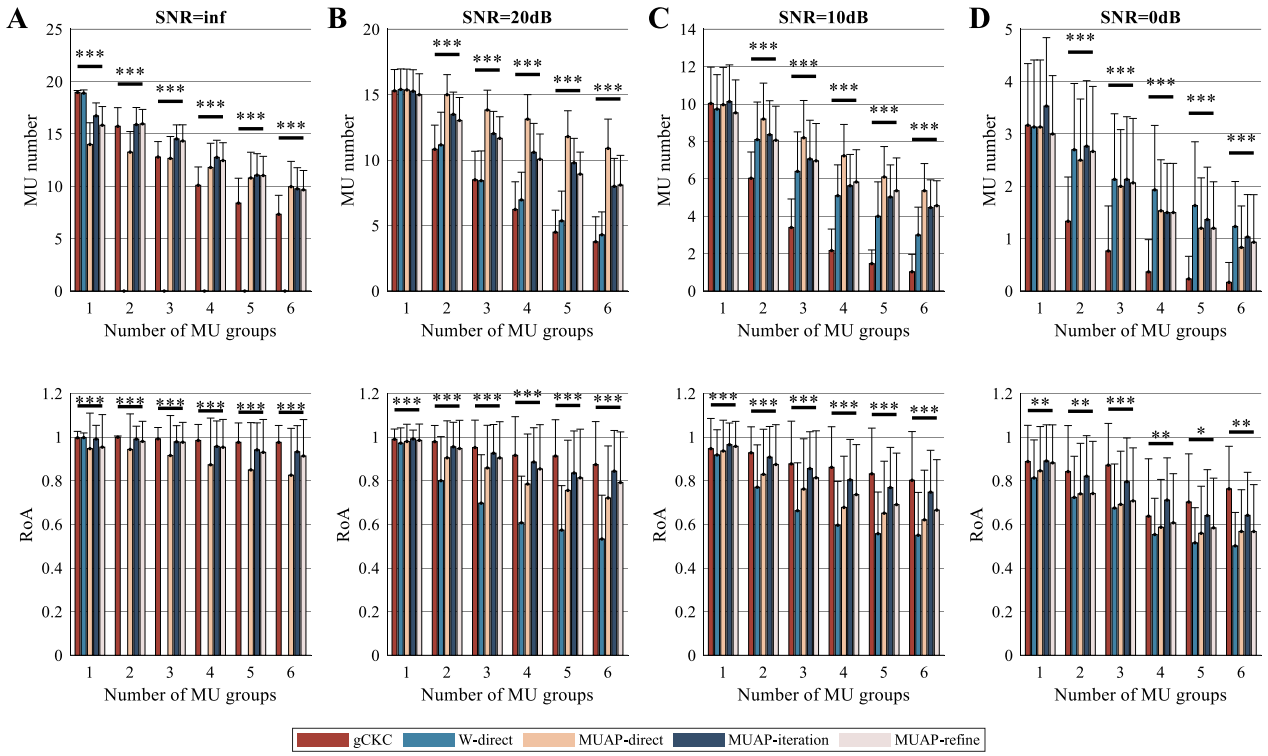

Fig. 5 The decomposition results when using different decomposition methods. **A-D** illustrates the number of identified MUs and their RoA during the simulated condition without noise and with SNR of 20 dB, 10 dB, and 0 dB, respectively. The number in the horizontal axis indicates how many MU groups were involved when generating EMG signals. The symbol $***$ indicates the significant level of $P < 0.001$

of identified MUs drops dramatically with the increase of the extending factor.

Experimental validation

Figure 8 shows the results of the experimental validation. Figure 8A and B depict the torque signals and corresponding decomposed MUSTs during four wrist movements. The MUAP-based method identified significantly more MUs than the classic method across all subjects (96±49 vs. 15±7) and movements (Figs. 8C and D). The improvement was most pronounced during combination movements, where the complexity of signals was higher. When decomposing the EMG signals of multiple contraction levels, the MUAP-based method also obtained more MUSTs (145±93) than gCKC (51±26), as shown in Fig. 8F.

Discussion

Overall, the proposed MUAP-based decomposition method demonstrated superior performance in terms of accuracy, reliability, and computational efficiency, highlighting its potential for clinical and research applications.

Effect of intermediate steps in decomposition

The intermediate steps involved in the MUAP-based decomposition method play a crucial role in determining the overall accuracy and efficiency of the process. Our study assessed various factors, such as MU filter reconstruction methods, EMG covariance matrices, MUAP extraction techniques, and extending factors, to understand their impact on decomposition performance.

MUAPs represent the electrical activity of individual MUs and can be used for EMG decomposition [39]. As the length of MU filters is limited, how to extract the most representative information about the unique spatial distribution is important. The results demonstrated that selecting the optimal reconstruction method can significantly enhance MU identification accuracy. The Maximum PPV method was found to yield the highest number of identified MUs and the best RoA compared to other methods like Centered Spike and Maximum Product (Fig. 4A). The primary reason may be attributed to the fact that waveform amplitude fluctuates most noticeably near the maximum absolute value, thereby best reflecting the propagation properties. The Maximum PPV or product method could also extract related information as the suboptimal performance was obtained. Directly extracting the samples from the waveform center is not

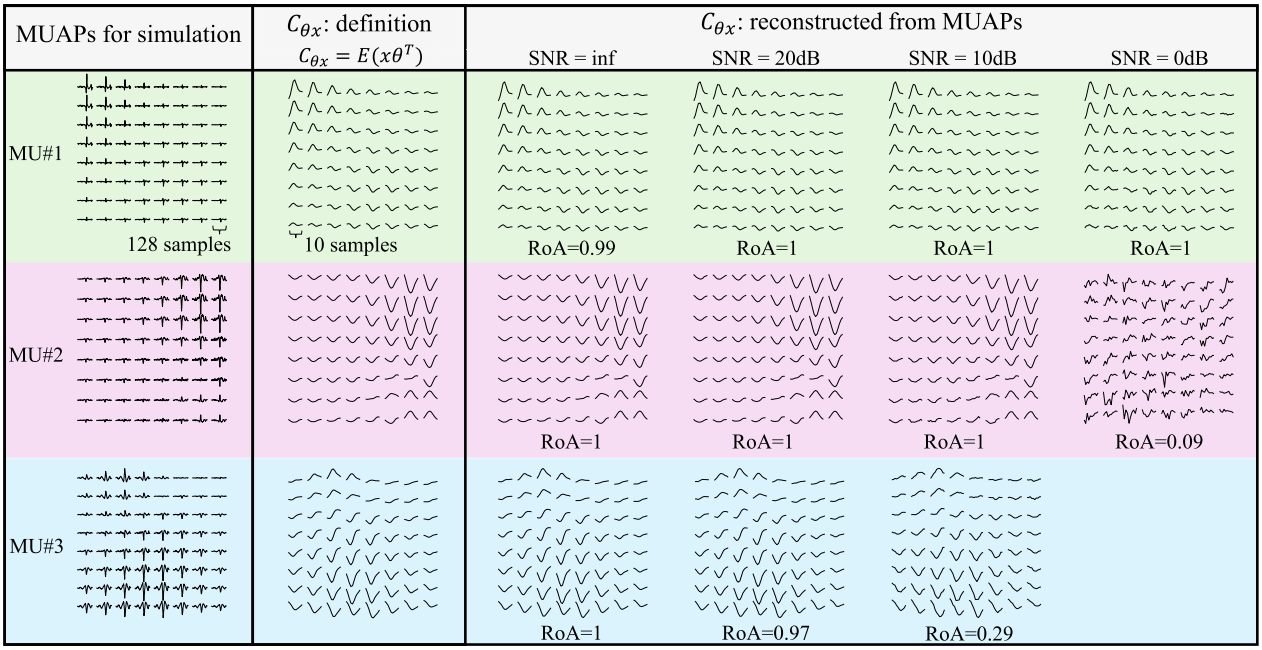

Fig. 6 Three example MUAPs and reconstructed MU filters. Each row displays information corresponding to the same MU. The left column illustrates the 64-channel MUAPs for simulation. Each channel contains 128 samples (62.5 ms). The middle column gives the MU filter estimated based on the definition, which was the cross-correlation between EMG signals and MUSTs. The EMG signals used for estimation were noise-free. The right column shows the MU filters reconstructed by Centered Peak under different noise conditions. The RoA gives the accuracy of identified MUST when using the reconstructed MU filter to decompose EMG signals. We arranged the waveforms of the MU filters according to channel positions, with each channel containing 10 samples. The missing MU filter for MU3 at 0 dB SNR is due to the inability to identify the MUST

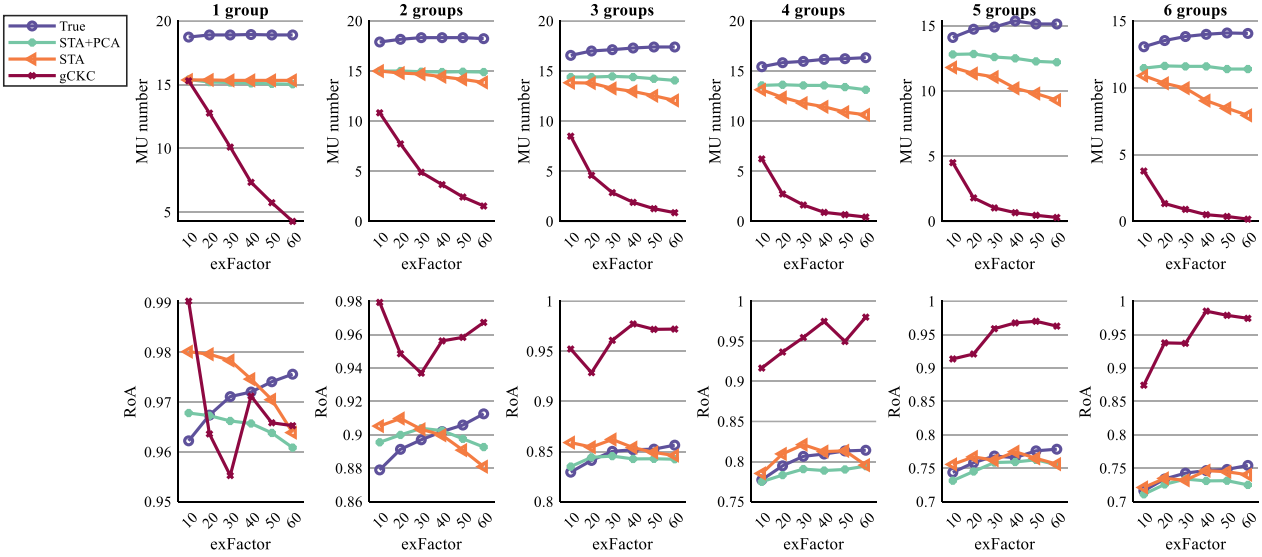

Fig. 7 The effect of extending factors (exFactor) on the decomposition results when different numbers of MU groups were involved. The MU filters were reconstructed from MUAPs (true, STA+PCA, or STA) with a length of exFactor using the Centered Peak method. For the gCKC method, the decomposition was implemented by extending the EMG signals with corresponding factors. The decomposition results were obtained based on the simulated signals with an SNR of 20 dB

advisable since the pulse trains for STA might have random shifts caused by signal extending.

Among the tested covariance matrices, the Current Cxx method significantly outperformed Raw Cxx regarding MU identification and RoA (Fig. 4B). This highlights the importance of using the most relevant and immediate data for constructing covariance matrices, which can improve the decomposition accuracy. The global Cxx obtained comparable performance with the current Cxx, indicating the possible existence of a common Cxx. The methods to extract MUAPs had little effect on the decomposition, as the MU number and the RoA obtained by STA and LS showed no significant difference.

The impact of extending factors on decomposition performance was significant, with optimal results observed at specific values (Fig. 7). For MU filters reconstructed from MUAPs using the Centered Peak method, performance improved with increasing extending factors up to a point, after which the benefits plateaued. This indicates that selecting appropriate extending factors is crucial for maximizing the method's effectiveness [25]. It should be noted that when the ground-truth MUAP was used, the decomposition performance always increased with the extending factor. This indicates that there is still some error between the estimated MUAP and the true value, and reducing this error has the potential to further improve the decomposition performance based on MUAP.

Reconstructing a MU filter using MUAP is challenging, and improper MUAP extraction can significantly affect the reconstruction process and following decomposition. In this study, we tested different MU filter reconstruction methods, among which the Centered Peak method yielded the best results, and we recommend it as the preferred approach. Two MUAP extraction methods were tested, but no significant difference was observed between them. Apart from the MUAP extraction method, the quality of MUAP estimation is also influenced by the decomposition accuracy of MUST, which is determined by EMG decomposition algorithms. These findings indicate that careful consideration and optimization of reconstruction steps and original CKC algorithms are essential for enhancing the performance of MUAP-based decomposition methods.

Performance comparison with traditional methods

The MUAP-based decomposition method shows significant improvements over the traditional CKC method. The MUAP-based method identified more MUs than traditional methods (Fig. 5), especially when additional MU groups were involved. This can be attributed to the distinct shapes and firing patterns of MUAPs, which facilitate more precise MU identification. When more than one groups were activated concurrently, the conventional CKC could only identify a small portion (<50%) of the MU group under most conditions. With the increase in the number of MU groups, the decomposition performance of CKC degraded rapidly. The separation matrix obtained based on the EMG signals of one MU group also failed to decompose the EMG signals with more MU groups. As the number of activated MUs increases, the complexity of the EMG signal rises, making it challenging to identify MUSTs and extract MUAPs accurately. As a result, a decline was also observed in the performance of the proposed method when involved MU groups increased (Fig. 5). However, the MUAP-based method showed superior decomposition when more MU groups were involved. The MUAP-direct identified more than half of the MUs of each group even when six MU groups were involved (under SNR 20 dB).

Therefore, the MUAP-based method showed the ability to consistently identify and track motor unit discharges across different decompositions and EMG conditions. Traditional BSS-based techniques often struggle with consistency, leading to unreliable motor unit tracking, especially in multi-DoF movements [40]. In this study, directly decomposing multi-DoF EMG signals, where a large number of MUs were activated, results in few identifiable MUs. However, by first decomposing single-DoF EMG signals (with fewer activated MUs) to construct MU filters and then integrating the MU filters for multi-DoF EMG decomposition, the number of identified MU is significantly improved (Fig. 8). When performing EMG decomposition across multiple contraction levels, the MUAP-based method consistently demonstrated superior performance to traditional methods, identifying many more MUSTs that were highly correlated with the contraction intensity. During the decomposition of low-force EMG signals, several MU filters reconstructed from high-force EMG signals became ineffective, as the corresponding MUs were not activated. However, the MU filters reconstructed from low-force EMG signals generally remained effective for higher force levels (e.g., 90% MVC), thereby increasing the number of identified MUSTs and demonstrating the effectiveness and superiority of the MU filter reconstruction approach. The MUAP method, by leveraging the unique characteristics of MUAPs, provides more reliable tracking of motor units, which is essential for accurate longitudinal studies and applications where consistent MU identification is crucial.

Similar to previous studies [17, 41], the signal quality had a dramatic effect on the decomposition performance for all the tested methods. With the increased noise level,

Table 1 The time cost of different decomposition methods. The time unit is second and calculated when decomposing 12-second signals

Extending factor	MUAP-direct	MUAP-refine	MUAP-iteration	gCKC
10	1.00±0.17	21.57±4.43	51.00±8.27	106.90±12.42
20	1.00±0.17	24.28±5.05	86.33±16.15	161.45±16.74
30	1.03±0.17	25.23±5.59	118.01±19.80	217.40±24.23
40	1.02±0.16	26.61±5.68	152.84±30.55	277.41±39.87
50	1.05±0.17	28.50±6.29	227.58±39.20	420.62±35.75
60	1.06±0.15	29.51±6.20	265.88±43.24	484.77±41.67

fewer MUs were identified, and the RoA decreased. This is mainly due to the failure of MU filter reconstruction. On the one hand, the CKC method fails under low SNR conditions, making it difficult to identify MUSTs. On the other hand, the estimation of MUAPs is also compromised as the noise increases [28], as shown in Fig. 6. For the three MUAP-based decomposition ways, the MUAP-iteration or MUAP-refine could improve the decomposition accuracy, but at the cost of identified MUs quantity and computation complexity. The MUAP-direct approach exhibited significantly lower time costs compared to iterative methods like the other two MUAP-based methods and gCKC (Tab. 1). Moreover, the time consumption of MUAP-direct showed nearly no increase as the extending factor grew. This efficiency is crucial for real-time applications, such as neurorehabilitation and prosthetic control, where timely processing is essential.

The proposed MUAP-based decomposition method is built upon the CKC algorithm framework, reconstructing MU filters from MUAPs for EMG decomposition. In

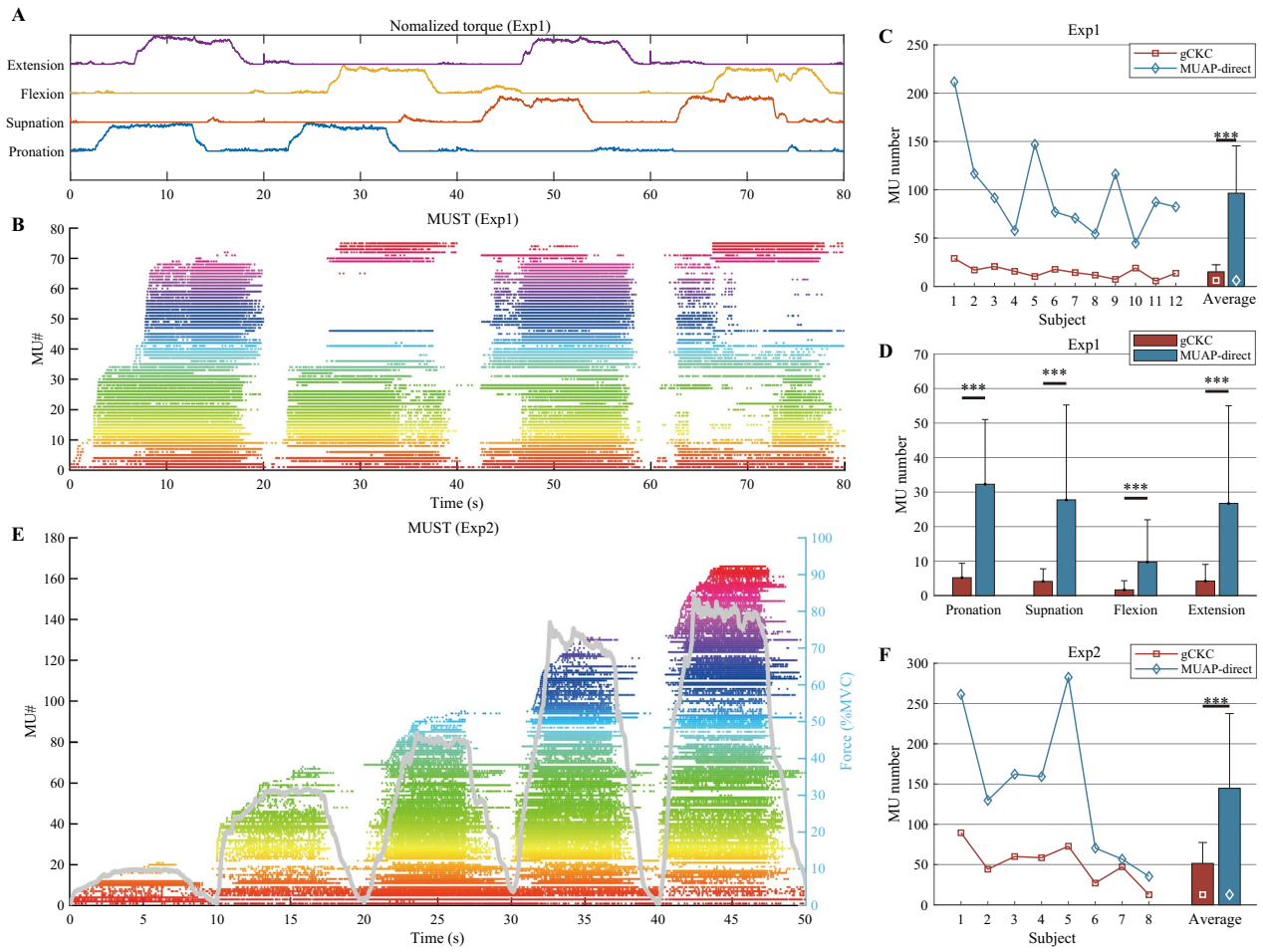

Fig. 8 The decomposition results of experimental signals. **A** shows the torque signals of four movements concurrently recorded with EMG signals in the first experiment (Exp1). The decomposed MUSTs by MUAP-direct are illustrated in **B**. **C** and **D** give the decomposition results of each subject and each motion when using the classic and MUAP-based methods. **E** and **F** illustrate the example MUSTs decoded by MUAP-direct and the decomposition results of all subjects in the second experiment (Exp2). The gray line in E indicates the force signals. The symbol *** indicates the significant level of $p<0.001$. The extending factor was set to 10

previous studies [9, 25, 42][43], the MU filters are typically a set of parameters iteratively estimated, and these parameters are influenced by the EMG signals used for decomposition. In contrast, extracting MU filters from MUAPs requires less complex computation and offers greater interpretability. In the simulation test, when using ground-truth MUAPs to reconstruct MU filters for EMG decomposition, the performance was significantly improved compared to using MUAP estimates, further proving the great potential of the proposed method. In other EMG decomposition algorithms, such as fastICA, the EMG signals undergo transformations like whitening, making it less feasible to extract separation vectors from MUAPs directly. However, this represents a promising direction for future research to enhance the performance of ICA-based decomposition algorithms.

Applications and limitations

The enhanced performance of the MUAP-based decomposition method has several implications for clinical and research applications, as well as some limitations to consider. Improved accuracy and robustness in MU identification can lead to more reliable diagnostics for neuromuscular disorders [6, 44]. Accurate tracking of MU activities over time can aid in monitoring disease progression and evaluating treatment efficacy. The method's efficiency and reliability make it suitable for real-time applications, such as controlling prosthetic limbs or providing feedback in neurorehabilitation settings [45].

It should be noted that the MUAP-based decomposition was proposed based on the assumption of unique MUAP distribution. If the two MUAPs were highly similar, such as from reinnervated muscles, the proposed method might fail to identify their discharge trains accurately. The sensitivity to the similarity of MUAP distributions is worth exploring in future work. As to the reconstruction method of the MU filter, while the STA method showed superior performance, the choice of extraction technique can influence decomposition results. Further research is needed to optimize these techniques to reduce the error between the estimated MUAPs and ground truth. Although validated with both simulated and experimental datasets, additional validation with diverse datasets and in different experimental setups is necessary to generalize the findings. In addition, only indirect metrics such as PNR, CoV, and correlation with kinetics were adopted for decomposition evaluation. It will be necessary to conduct invasive experiments, for example, recording the intramuscular and surface EMG signals concurrently [38–46], to provide more direct and comprehensive validation of the proposed decomposition methods for surface EMG signals.

Conclusion

In this study, we proposed a MUAP-based decomposition method upon the CKC algorithm, reconstructing MU filters directly from MUAPs. The MUAP-based method offers significant advancements in simulated and experimental EMG decomposition, providing improved accuracy and efficiency over traditional techniques. Its ability to track motor units reliably and process data in real-time highlights its potential for various applications, including clinical diagnostics, neurorehabilitation, prosthetic control, and motor control research. Further optimization and extensive validation are necessary to fully harness its capabilities and address any limitations.

Abbreviations

BSS	Blind source separation
CKC	Convolution Kernel compensation
CoV	Coefficient of variation
Current Cxx	Covariance matrix calculated by EMG signals to be decomposed
EMG	Electromyography
fastICA	Fast independent component analysis
gCKC	With a natural gradient descent iteration
Global Cxx	Covariance matrix calculated by all EMG signals
ISI	Inter-spike interval
LS	Least square, method to extract MUAP
MU	Motor unit
MUAP	Motor unit action potential
MUST	Motor unit spike train
MVC	Maximum voluntary contraction
PCA	Principal component analysis
PNR	Pulse-to-noise ratio
PPV	Peak-to-peak value
Raw Cxx	Covariance matrix calculated by EMG signals from which the MU filters are reconstructed
RoA	Rate of agreement
SNR	Signal-to-noise ratio

Author contributions

CC and DL designed and participated in all the data collection and analysis processes, and MX participated in the data collection and analysis processes of the second experiment. CC wrote the main manuscript, and all the authors reviewed it.

Funding

This work was funded by the National Natural Science Foundation of China (Grant Nos. 52205024 and 52227808).

Data availability

The codes and data used for the results presented in this study are available from the corresponding author upon reasonable request.

Declarations

Ethics approval and consent to participate

The experiments undertaken within this manuscript were approved by the local ethics committee of Shanghai Jiao Tong University (approval number B2020026I) and followed the Declaration of Helsinki. Prior to the subjects participating in the experiment, written consent was given.

Consent for publication

Not applicable.

Competing interests

The authors declare no Conflict of interest.

Received: 14 August 2024 Accepted: 28 February 2025
Published online: 14 March 2025

References

1. Farina D, Aszmann O. Bionic limbs: Clinical reality and academic promises. Sci Transl Med. 2014;6(257):257–1225712.
2. Heckman CJ, Enoka RM. Motor unit. Compr Physiol. 2012;2(4):2629–82.
3. Farina D, Vujaklija I, Sartori M, Kapelner T, Negro F, Jiang N, Bergmeister K, Andalib A, Principe J, Aszmann OC. Man/machine interface based on the discharge timings of spinal motor neurons after targeted muscle reinnervation. Nat Biomed Eng. 2017;1(2):0025.
4. Hu X, Rymer WZ, Suresh NL. Assessment of validity of a high-yield surface electromyogram decomposition. J Neuroeng Rehabil. 2013;10(1):99.
5. Del Vecchio A, Jones RHA, Schofield IS, Kinfe TM, Ibáñez J, Farina D, Baker SN. Interfacing motor units in nonhuman primates identifies a principal neural component for force control constrained by the size principle. J Neurosci. 2022;42(39):7386–99.
6. Farina D, Negro F, Dideriksen JL. The effective neural drive to muscles is the common synaptic input to motor neurons. J Physiol. 2014;592(Pt 16):3427–41.
7. Chen C, Yu Y, Sheng X, Farina D, Zhu X. Simultaneous and proportional control of wrist and hand movements by decoding motor unit discharges in real time. J Neural Eng. 2021;18(5): 056010.
8. Holobar A, Farina D. Blind source identification from the multichannel surface electromyogram. Physiol Meas. 2014;35(7):143.
9. Holobar A, Zazula D. Multichannel blind source separation using convolution kernel compensation. IEEE Trans Signal Process. 2007;55(9):4487–96.
10. Chen M, Zhang X, Chen X, Zhou P. Automatic implementation of progressive fastica peel-off for high density surface EMG decomposition. IEEE Trans Neural Syst Rehabilit Eng. 2018;26(1):144–52.
11. Negro F, Muceli S, Castronovo AM, Holobar A, Farina D. Multi-channel intramuscular and surface EMG decomposition by convolutive blind source separation. J Neural Eng. 2016;13(2): 026027.
12. Holobar A, Zazula D. Correlation-based decomposition of surface electromyograms at low contraction forces. Med Biol Eng Comput. 2004;42(4):487–95.
13. Glaser V, Holobar A. Motor unit identification from high-density surface electromyograms in repeated dynamic muscle contractions. IEEE Trans Neural Syst Rehabilit Eng. 2019;27(1):66–75.
14. Chen M, Zhang X, Zhou P. A novel validation approach for high-density surface EMG decomposition in motor neuron disease. IEEE Trans Neural Syst Rehabilit Eng. 2018;26(6):1161–8.
15. Chen M, Zhang X, Lu Z, Li X, Zhou P. Two-source validation of progressive fastica peel-off for automatic surface EMG decomposition in human first dorsal interosseous muscle. Int J Neural Syst. 2018;28(09):1850019.
16. Chen C, Ma S, Sheng X, Farina D, Zhu X. Adaptive real-time identification of motor unit discharges from non-stationary high-density surface electromyographic signals. IEEE Trans Biomed Eng. 2020;67(12):3501–9.
17. Chen M, Zhou P. A n ovel method for h igh d ensity s urface emg d ecomposition b ased on k ernel c onstrained fastica and c orrelation c onstrained fastica. IEEE Trans Neural Syst Rehabilit Eng. 2024;2:1–1.
18. Muceli S, Poppendieck W, Holobar A, Gandevia S, Liebetanz D, Farina D. Blind identification of the spinal cord output in humans with high-density electrode arrays implanted in muscles. Sci Adv. 2022;8(46):5040.
19. Martinez-Valdes E, Negro F, Laine CM, Falla D, Mayer F, Farina D. Tracking motor units longitudinally across experimental sessions with high-density surface electromyography. J Physiol. 2017;595(5):1479–96.
20. Del Vecchio A, Casolo A, Negro F, Scorcelletti M, Bazzucchi I, Enoka R, Felici F, Farina D. The increase in muscle force after 4 weeks of strength training is mediated by adaptations in motor unit recruitment and rate coding. J Physiol. 2019;597(7):1873–87.
21. De Luca CJ, Chang S-S, Roy SH, Kline JC, Nawab SH. Decomposition of surface EMG signals from cyclic dynamic contractions. J Neurophysiol. 2014;113(6):1941–51.
22. Kramberger M, Holobar A. On the prediction of motor unit filter changes in blind source separation of high-density surface electromyograms during dynamic muscle contractions. IEEE Access. 2021;9:103533–40.
23. Francic A, Holobar A. On the reuse of motor unit filters in high density surface electromyograms recorded at different contraction levels. IEEE Access. 2021;9:115227–36.
24. Merletti R, Farina D. Surface EMG Decomposition, 2016;180–209
25. Chen C, Ma S, Yu Y, Sheng X, Zhu X. Segment-wise decomposition of surface electromyography to identify discharges across motor neuron populations. IEEE Trans Neural Syst Rehabilit Eng. 2022;30:2012–21.
26. Zheng Y, Hu X. Real-time isometric finger extension force estimation based on motor unit discharge information. J Neural Eng. 2019;16(6): 066006.
27. Holobar A, Zazula D. Gradient convolution kernel compensation applied to surface electromyograms. In: International Conference on Independent Component Analysis and Signal Separation, 2007;617–624 Springer
28. Kay SM. Fundamentals of Statistical Signal Processing: Estimation Theory. USA: Prentice-Hall Inc; 1993;
29. Farina D, Cescon C, Negro F, Enoka RM. Amplitude cancellation of motor-unit action potentials in the surface electromyogram can be estimated with spike-triggered averaging. J Neurophysiol. 2008;100(1):431–40.
30. Henneman E. Relation between size of neurons and their susceptibility to discharge. Science. 1957;126(3287):1345–7.
31. Fuglevand AJ, Winter DA, Patla AE. Models of recruitment and rate coding organization in motor-unit pools. J Neurophysiol. 1993;70(6):2470–88.
32. Chen C, Yu Y, Sheng X, Zhu X. Non-invasive analysis of motor unit activation during simultaneous and continuous wrist movements. IEEE J Biomed Health Inform. 2022;26(5):2106–15.
33. Xia M, Chen C, Sheng X, Ding H. Integration of motor unit filters for enhanced surface electromyogram decomposition during varying force isometric contraction. IEEE Trans Neural Syst Rehabilit Eng. 2024;32:2905–13.
34. Xia M, Chen C, Xu Y, Li Y, Sheng X, Ding H. Extracting individual muscle drive and activity from high-density surface electromyography signals based on the center of gravity of motor unit. IEEE Trans Biomed Eng. 2023;70(10):2852–62.
35. Chen C, Ma S, Sheng X, Zhu X. A peel-off convolution kernel compensation method for surface electromyography decomposition. Biomed Signal Process Control. 2023;85: 104897.
36. Lundsberg J, Björkman A, Malesevic N, Antfolk C. Inferring position of motor units from high-density surface emg. Sci Rep. 2024;14(1):3858.
37. Ning Y, Zhu X, Zhu S, Zhang Y. Surface EMG decomposition based on k-means clustering and convolution kernel compensation. IEEE J Biomed Health Inf. 2015;19(2):471–7.
38. Holobar A, Minetto MA, Botter A, Negro F, Farina D. Experimental analysis of accuracy in the identification of motor unit spike trains from high-density surface EMG. IEEE Trans Neural Syst Rehabilit Eng. 2010;18(3):221–9.
39. Merletti R, Farina D. Biophysics of the Generation of EMG Signals, 2016;1–24
40. Kapelner T, Negro F, Aszmann OC, Farina D. Decoding motor unit activity from forearm muscles: Perspectives for myoelectric control. IEEE Trans Neural Syst Rehabilit Eng. 2018;26(1):244–51.
41. Xu Y, Yu Y, Xia M, Sheng X, Zhu X. A novel and efficient surface electromyography decomposition algorithm using local spatial information. IEEE J Biomed Health Inf. 2023;27(1):286–95.
42. Avrillon S, Hug F, Gibbs C, Farina D. Tutorial on muedit: An open-source software for identifying and analysing the discharge timing of motor units from electromyographic signals. BioRxiv. 2023;77:0713548568.
43. Klotz T, Lehmann L, Negro F, Röhrle O. High-density magnetomyography is superior to high-density surface electromyography for motor unit decomposition a simulation study. J Neural Eng. 2023;20:4.
44. Holobar A, Glaser V, Gallego JA, Dideriksen JL, Farina D. Non-invasive characterization of motor unit behaviour in pathological tremor. J Neural Eng. 2012;9(5): 056011.
45. Formento E, Botros P, Carmena JM. Skilled independent control of individual motor units via a non-invasive neuromuscular-machine interface. J Neural Eng. 2021;18(6): 066019.
46. Grison A, Pereda JI, Muceli S, Kundu A, Baracat F, Indiveri G, Donati E, Farina D. Intramuscular high-density micro-electrode arrays enable high-precision decoding and mapping of spinal motor neurons to reveal hand control. arXiv preprint arXiv:2410.11016 2024;